# Electrical Performance of Silicon-on-Insulator Field-Effect Transistors with Multiple Top-Gate Organic Layers in Electrolyte Solution

**Bassam Khamaisi,[†,¶] Oshri Vaknin,[‡,¶] Oren Shaya,[†] and Nurit Ashkenasy[§,⊥,*]**

[†]School of Electrical Engineering, Faculty of Engineering, Tel-Aviv University, Ramat-Aviv, Israel, 69978, [‡]Department of Bio-Medical Engineering, [§]Department of Materials Engineering, and [⊥]The Ilze Katz Institute for Nanoscience and Nanotechnology, Ben-Gurion University of the Negev, Beer-Sheva, Israel, 84105. [¶]These authors contributed equally to this work.

**ABSTRACT** The utilization of field-effect transistor (FET) devices in biosensing applications have been extensively studied in recent years. Qualitative and quantitative understanding of the contribution of the organic layers constructed on the device gate, and the electrolyte media, on the behavior of the device is thus crucial. In this work we analyze the contribution of different organic layers on the pH sensitivity, threshold voltage, and gain of a silicon-on-insulator based FET device. We further monitor how these properties change as function of the electrolyte screening length. Our results show that in addition to electrostatic effects, changes in the amphoteric nature of the surface also affect the device threshold voltage. These effects were found to be additive for the first (3-aminopropyl)trimethoxysilane linker layer and second biotin receptor layer. For the top streptavidin protein layer, these two effects cancel each other. The number and nature of amphoteric groups on the surface, which changes upon the formation of the layers, was shown also to affect the pH sensitivity of the device. The pH sensitivity reduces with the construction of the first two layers. However, after the formation of the streptavidin protein layer, the protein's multiple charged side chains induce an increase in the sensitivity at low ionic strengths. Furthermore, the organic layers were found to influence the device gain due to their dielectric properties, reducing the gain with the successive construction of each layer. These results demonstrate the multilevel influence of organic layers on the behavior of the FET devices.

**KEYWORDS:** biosensor · field effect transistor · silicon on insulator · organic layers · pH sensitivity · threshold voltage · gain · Debye screening length

Field effect transistor biosensors (bio-FETs) have received considerable attention due to their ability to transduce biological recognition events directly to an electrical signal.[1,2] Sensing occurs in these devices by changes in the transistor's channel conductivity, induced by the binding of analyte biomolecules to receptor molecules on the floating gate of the device. These effects include changes in the device's surface-band bending due to the molecules' effective charge,[3] and changes in the oxide surface work function due to the layer molecular dipole,[4,5] which thus may alter the flat band voltage and consequently the threshold voltage of the device. The sensitivity of the FETs' channel conductivity to these effects makes this type of biosensors very attractive, providing a comprehensive and efficient method for detecting a wide variety of biomolecules.[6,7] However, these effects may be attenuated by redistribution of mobile ions in the intermolecular spaces within the adsorbed molecular layers[8] and depolarization of the layers' dipole due to the very large electric fields induced in the layers,[4,5,9] limiting the magnitude of the obtained signal.

Since the sensitivity of the sensor is a critical parameter, large surface-to-volume ratio devices based on semiconductor nanowires[10,11] and carbon nanotubes[12] have been commonly utilized as the device channel. However, in recent years complementary metal oxide semiconductor (CMOS) based technologies have been applied for successful fabrication of high performance bio-FETs on silicon-on-insulator (SOI) wafers,[13] eliminating the need for using 'bottom up' techniques in the fabrication process. The operation principals of SOI-based devices are similar to that of conventional FETs.[14] However, the buried oxide layer enables additional gating of the device by applying a potential through a fourth bottom electrode. It has been recently shown that when such devices are used in depletion mode, charge-coupling effects may increase the sensitivity of the sensor.[15,16] Despite the promising potential and advantages, quantitative estimation of the modulation of device performance, and their correlation with the attached organic layers' properties has not yet, to the best of our knowledge, been evaluated. In this work, we combine macroscopic

*Address correspondence to nurita@bgu.ac.il.

Received for review April 29, 2010 and accepted July 13, 2010.

**Published online July 22, 2010.**
10.1021/nn100936h

current−voltage ($I-V$) measurements of SOI bio-FET devices, with an appropriate device modeling, in order to obtain a quantitative estimation of changes in device behavior following the formation of organic layers on top of the device gate, in an aqueous environment. To achieve this goal we monitor changes in the pH sensitivity, threshold voltage, $V_{th}$, and device gain after the formation of linker, receptor, and analyte layers on top of the device floating gate, using (3-aminopropyl)trimethoxysilane (APTMS), which is a widely used linker, and streptavidin−biotin as antigen/antibody model system. Our results suggest a decrease in the pH sensitivity with the successive introduction of small organic molecules to the gate surface; however, this sensitivity may increase upon the adsorption of multiply charged proteins. By analyzing changes in $V_{th}$, we follow the contribution of the organic layers both by affecting the point of zero charge (PZC) of the surface, and dipolar effects. The influence of the solution ionic strength on these effects is studied, demonstrating an increased sensitivity to the top protein layer with decreasing ionic strength. Finally, we show that the device gain decreases during the construction of the bio-organic layers due to capacitive effects.

## DEVICE MODELING

In fully depleted SOI-FET devices the back gate voltage, $V_{BG}$, can be used for opening the device's channel, making it possible to keep the top gate dielectric exposed, and thus available for the binding of molecular layers, which are necessary for the device sensing process. In this configuration the layers are bound to a top, nanometric thick, silicon oxide surface, thus imposing large gating effects by the molecules. These effects can be monitored by their influence on the back gate threshold voltage, $V_{th\text{-}BG}$. The modeling of these effects was carried out for a four-terminal enhancement $n$-channel SOI device configuration (Figure 1a). A one-dimensional analysis was developed, combining a fully depleted SOI model in order to test the electrostatic influence of the different organic layers,[7,17] and an electrolyte insulator semiconductor (EIS) model in order to study the effect of the surrounding electrolyte media.[18−21] Accordingly, the potential distribution, $\Phi$, between the back gate of the device and a reference electrode in solution, which can also be referred to as a front electrode, was obtained by solving the one-dimensional Poisson's equation (Figure 1b):

$$\frac{d^2\Phi(x)}{dx^2} = \frac{qN_a}{\varepsilon_{Si}}, \quad 0 \le x \le t_{Si} \tag{1}$$

using the following boundary conditions:

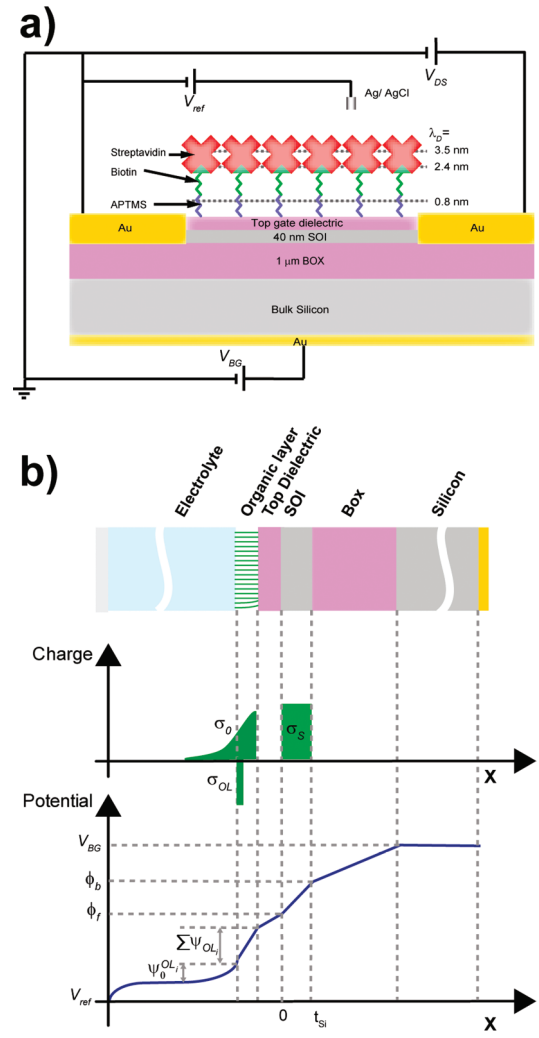


**Figure 1. (a) Schematic of SOI bioFET and electronic characterization setup (not to scale). (b) Schematic illustration of potential and charge distribution across the device layers (for $V_{ref} = 0$), showing the different parameters used in the 1-D electrostatic potential (details are in the text).**

$$\Phi(0) = \Phi_f, \frac{d\Phi(x)}{dx}_{x=0} = \frac{\varepsilon_{ox}}{\varepsilon_{Si}} \frac{\Phi_f - (V'_{ref} + \Psi_0^{OL_i} - \sum_i \Psi_{OL_i})}{t_{ox}} \tag{2}$$

$$\Phi(t_{Si}) = \Phi_b, \frac{d\Phi(x)}{dx}_{x=t_{Si}} = \frac{\varepsilon_{ox}}{\varepsilon_{Si}} \frac{V'_{BG} - \Phi_b}{t_{Box}} \tag{3}$$

where $q$ is the electronic charge, $N_a$ is the channel doping concentration, and $\varepsilon_{Si}$ and $\varepsilon_{ox}$ are the permittivities of silicon and silicon-oxide, respectively. $\Phi_f$ and $\Phi_b$ are the potentials at the front and back oxide−SOI interface, respectively. The effective front and back gate potentials were defined by $V'_{ref} = V_{ref} - V^f_{FB}$ and $V'_{BG} = V_{BG} - V^b_{FB}$, respectively, where $V_{ref}$ and $V_{BG}$ are the front- and back-gate potentials, and $V^f_{FB}$ is the flat-band voltage at the front side of the SOI channel, which includes constant parameters of the electrolyte. $V^b_{FB}$ is the flat-band voltage at the

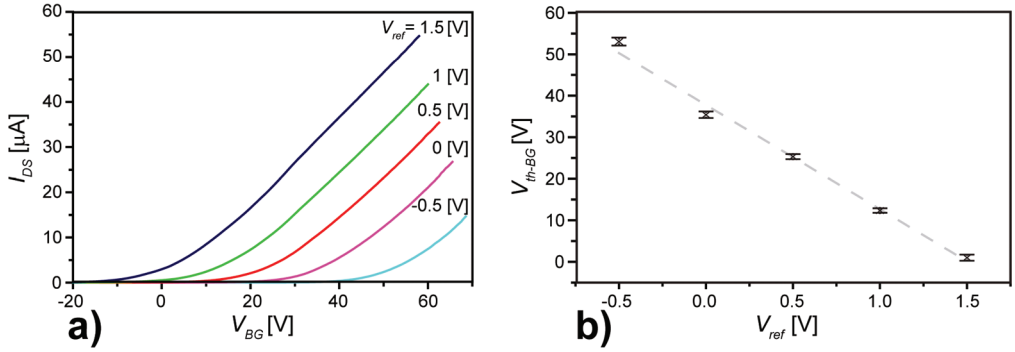


**Figure 2. (a) $I_{DS}-V_{BG}$ curves of a bare device as a function of $V_{ref}$ (data collected in solutions of 1X PBS buffer). (b) $V_{th\text{-}BG}$ dependence on $V_{ref}$. $V_{th\text{-}BG}$ values were extrapolated from the linear part of the corresponding $I_{DS}-V_{BG}$ curves. A linear dependence is observed for the experimental results (black crosses). The slope of a linear fit (dashed gray line, $R^2 = 0.989$) yields a coupling factor of 25 ± 1.**

back of the device. $\Psi_0^{OL_i}$ is the potential drop at the gate−liquid interface for organic layer $i$, and $\Psi_{OL_i}$ is the potential drop over the organic layer (Figure 1b). $t_{ox}$ and $t_{Box}$ are the front and buried oxide layer thicknesses, respectively, and $t_{Si}$ is the SOI layer thickness.

Charge conservation in the system, neglecting contributions from surface states and fixed or parasitic charges, requires that $\sigma_0 + \sigma_{OL} + \sigma_s = 0$, where $\sigma_0$ is the electrolyte Helmholtz double layer charge, $\sigma_{OL}$ is the organic layers effective charge, and $\sigma_s$ the space charge in the silicon (Figure 1b). Thus the solution of eq 1 for a bare device was obtained, neglecting the contribution of the organic layers to the boundary condition (2), and assuming the conventional threshold condition $\Phi_f \equiv 2\Phi_F = 2kT/q \ln(N_a/n_i)$, yielding

$$V_{th-BG_{Bare}} = V_{FB}^{b} + \frac{C_{Si}C_{ox}}{C_{Box}(C_{Si}+C_{ox})}\left[\frac{qN_a t_{Si}}{C_{ox}}\left(1+\frac{C_{ox}}{2C_{Si}}\right) - (V_{ref} - V_{FB}^{f} + \Psi_0^{Bare}) + 2\Phi_F\right] \quad (4)$$

where $C_{Box} \equiv \varepsilon_{ox}/t_{Box}$, $C_{ox} \equiv \varepsilon_{ox}/t_{ox}$, and $C_{Si} \equiv \varepsilon_{Si}/t_{Si}$.

Equation 4 shows a negative linear relation between the back-gate threshold voltage, $V_{th\text{-}BG}$, and $V_{ref}$, with $V_{th\text{-}BG}$ decreasing as $V_{ref}$ increases, with a coupling factor $f_C \equiv C_{Si}C_{ox}/(C_{Box}(C_{Si}+C_{ox}))$. This is in agreement with the metal oxide semiconductor FET (MOSFET) theory; a positive/negative $V_{ref}$ (similarly to a positive/negative voltage in MOSFET's gate) causes a hole depletion/accumulation in the SOI layer, consequently decreasing/increasing $V_{th\text{-}BG}$. After modification of the surface $V_{th\text{-}BG}$ becomes

$$V_{th-BG_i} = V_{FB}^{b} + \frac{C_{Si}C_{ox}}{C_{Box}(C_{Si}+C_{ox})}\left[\frac{qN_a t_{Si}}{C_{ox}}\left(1+\frac{C_{ox}}{2C_{Si}}\right) - (V_{ref} - V_{FB}^{f} + \Psi_0^{OL_i} - \sum_i \Psi_{OL_i}) + 2\Phi_F\right] \quad (5)$$

Thus the threshold voltage shift, $\Delta V_{th\text{-}BG_i}$, due to the chemical modification is

$$\Delta V_{th-BG_i} = f_C[\Psi_{OL_i} + \Delta\Psi_{0_i}] \quad (6)$$

where $\Delta\Psi_{0_i} \equiv \Psi_0^{OL_{i-1}} - \Psi_0^{OL_i}$, which is the difference between the point-of-zero-charge (PZC) of the surface before and following modification ($\Psi_0^{OL_i}|_{i=0}$ represents the bare surface).[22] Thus, the threshold voltage shift includes the contribution of both the potential change over the monolayer originating from the molecules' charge and dipole, and changes in the PZC of the surface. $\Delta\Psi_0$ can be evaluated using the site-binding model by[22]

$$\Delta\Psi_{0_i} = A_{OL_i}\cdot pH_{OL_i}^{pzc} - A_{OL_{i-1}}\cdot pH_{OL_{i-1}}^{pzc} \quad (7)$$

where $A_{OL_{i-1}}$ and $A_{OL_i}$ are the pH sensitivity factors, $pH_{OL_{i-1}}^{pzc}$ and $pH_{OL_i}^{pzc}$ are the PZC of the surfaces, before and after surface modification, respectively.

The validity of the model was verified by monitoring experimentally the dependence of $V_{th\text{-}BG}$ on $V_{ref}$. A negative shift of the $I_{DS}-V_{BG}$ curves of a bare device with increasing $V_{ref}$ was observed (Figure 2a), manifesting a decrease in $V_{th\text{-}BG}$, as expected. Indeed, a linear dependence of $V_{th\text{-}BG}$, estimated from these experiments, on $V_{ref}$ is obtained (Figure 2b). From these results $f_C$ was estimated to be 25 ± 1, in agreement with a value of 24.5, calculated using the manufacturer's cited thickness values.

## RESULTS AND DISCUSSION

The behavior of a SOI-FET device with a floating gate depends both on the solution conditions (pH and ionic strength), and on the presence of an effective charge and dipole on its surface. Thus, to study these effects bare devices, as well as devices after the deposition of the APTMS linker, biotin receptor and streptavidin analyte layers were measured at various solution conditions. From the resultant current voltage relations quantitative analyses of the different contributions to device performance were performed.

**pH Sensitivity.** It is well established that the FET behavior in solution depends on the pH of the solution due to protonation/deprotonation of amphoteric groups on the surface.[22] Since these effects depend on the properties of the surface and ligands bound to it, we have

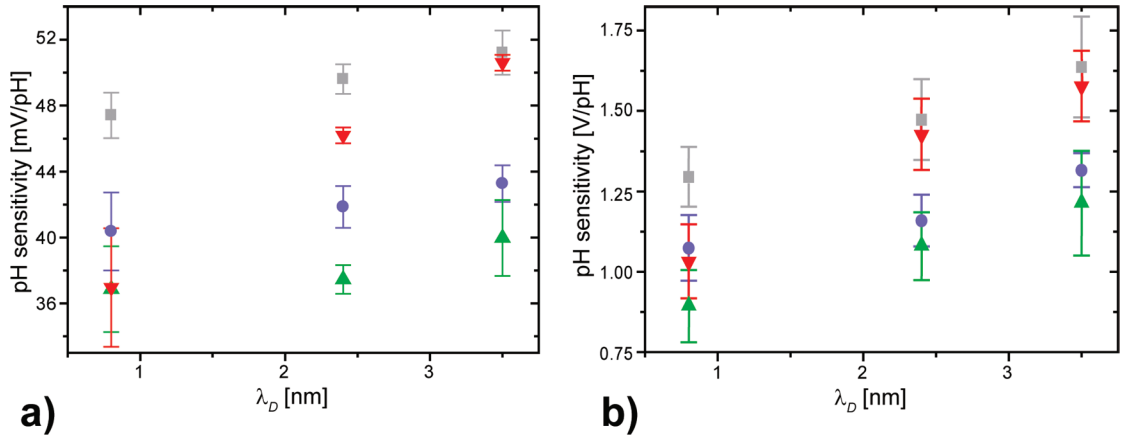


**Figure 3. pH sensitivity dependence on the solution screening length. Sensitivity was monitored using (a) $I_{DS}-V_{ref}$ ($V_{BG}$ = 30 V), and (b) $I_{DS}-V_{BG}$ ($V_{ref}$ = 1 V) curves in order to estimate $V_{th}$ for the different solutions' pH (see Methods section for details). Data for the bare device (gray square), and after APTMS (blue circle), biotin (green triangle), and streptavidin (red triangle) layers deposition is presented. The solution Debye screening length was calculated from the buffer ion concentration.[24]**

monitored the changes in the pH sensitivity, that is, the surface potential difference due to changes in the bulk solution pH, after each step of modification, at three different ionic strengths by the changes in $V_{th\text{-}ref}$ (Figure 3a). The results show that the highest pH sensitivity is obtained for the bare device. After APTMS monolayer formation the sensitivity decreases, in agreement with reported results.[23] A further decrease in the sensitivity is obtained after biotin binding. Interestingly, after binding of the large streptavidin molecule the sensitivity does not change for the large ionic strength; however, it increases at low ionic strength. Our results can be explained by the classic site-dissociation model developed by Van Hal *et al.*:[22]

$$\frac{\partial \Psi_0}{\partial pH_B} = -2.3\frac{kT}{q}\alpha, \quad \alpha \equiv \frac{1}{2.3\dfrac{kTC_{Diff}}{q^2\beta_{int}} + 1} \qquad (8)$$

where $k$ is the Boltzmann's constant, $T$ is the absolute temperature, $C_{Diff}$ is the differential double-layer capacitance, and $\beta_{int}$ is the intrinsic buffer capacity that depends on the total charge of amphoteric head groups. The parameter $\alpha$ is a dimensionless parameter that varies between 0 and 1. If $\alpha = 1$, the sensitivity reaches the Nernstian limit of 59.2 mV/pH at 298 K. Accordingly, the pH sensitivities of the bare device, which are above 48 mV/pH for the entire ionic strength range, are close to the Nernstian (ideal) sensitivity limit. This is probably due to the large density of OH groups on the surface that increase the value of $\beta_{int}$. The reduced sensitivity observed upon APTMS layer formation can, thus, be attributed to the formation of a mixed interface that is composed of two amphoteric groups: the Si−OH groups with p$K_a$ value of 6.8, and the APTMS amine head groups with p$K_a$ value of 9−10. This reduces the overall surface charge and thus $\beta_{int}$. Biotin binding to APTMS results in a decrease in the number of amine groups, thus decreasing the number of amphoteric sites. Finally, the increased sensitivity upon streptavidin binding can be explained by the large amount of amine and carboxylic side chains on the protein. These side chains reside outside the detection volume for the large ionic strength solution, as will be discussed below, thus not showing contribution to the sensitivity; however, for low ionic strength they become more dominant.

The slight decrease in the pH sensitivity with increasing buffer concentration for the same surface conditions shown in Figure 3 reflects changes in $C_{Diff}$. Since $C_{Diff}$ is a function of the ionic strength, a decrease in the ionic strength decreases $C_{Diff}$, which yields an increase in the pH sensitivity as deduced from eq 8. Since the pH sensitivity may affect device performance, it is important to take it into account in the analysis, as will be demonstrated below.

**$V_{th}$ Dependence on Organic Layers Formation.** To validate that the gate coupling effect demonstrated above applies also to changes in the surface−electrolyte interface potential, the pH sensitivity was evaluated by using the variations in $V_{th\text{-}BG}$ (Figure 3b). As expected, overall the same trends were observed, with the sensitivity values increasing by a factor of ~29, which is similar to the coupling factor that was obtained by varying $V_{ref}$. These results confirm that changes at the surface−electrolyte interface affect the back gate response in a similar fashion to changes in the front electrode potential. This allows us to correlate changes in $V_{th\text{-}BG}$ with the surface potential and quantify using the device coupling factor, as will be discussed below. Thus the use of a SOI-FET configuration allows us to study the effects of the organic layers' charge and dipole by monitoring the device back-gate threshold voltage. A small shift in the $I_{DS}-V_{BG}$ curve to lower $V_{BG}$ values is observed after the adsorption of the APTMS monolayer, with respect to the activated device (Figure 4a). This shift can be attributed to the addition of positive charge through the amine groups of the APTMS. After the con-

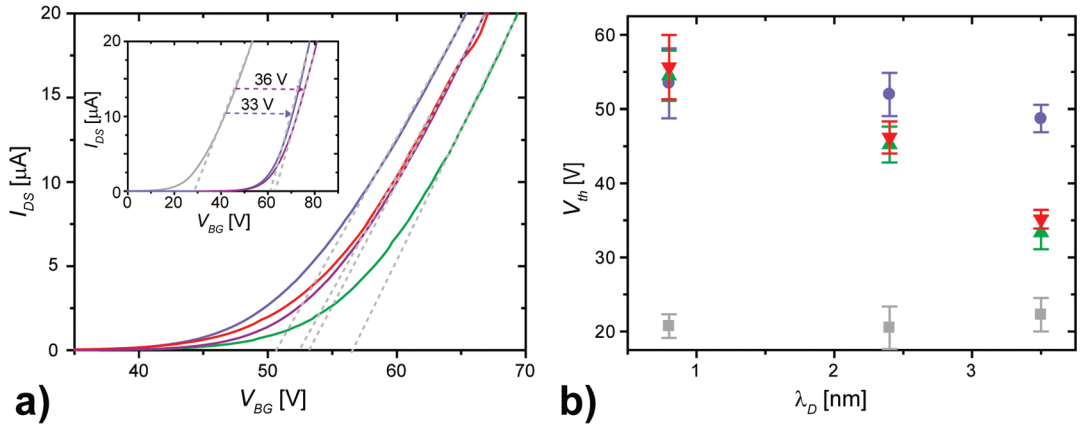


**Figure 4. $V_{th}$ dependence on organic layers and solution ionic strength. (a) $I_{DS}-V_{BG}$ curves of activated device (purple) and after APTMS (blue), biotin (green), and streptdavidin (red) layers (data collected in solutions of 1X PBS buffer, $\lambda_D$ = 0.8 nm). $V_{th}$ values were extrapolated from the linear part of each curve (marked by gray dashed lines). The $I_{DS}-V_{BG}$ curve of the bare gate is shown in the inset together with the curves of the gate after activation and APTMS deposition, showing the large effect of the activation process. The $V_{th\text{-}BG}$ shift of each curve with respect to the bare gate device is specified. (b) $V_{th\text{-}BG}$ as a function of the solution Debye screening length for the bare device (gray square), and after APTMS (blue circle), biotin (green triangle), and streptavidin (red triangle) layers deposition. ($V_{ref}$ = 0 V for all data in the figure).**

struction of the biotin layer the curve shifts to higher $V_{BG}$ values, and after streptavidin layer adsorption a small shift back to lower values is observed (Figure 4a). These shifts manifest changes in the $V_{th\text{-}BG}$ values.

Establishment of the influence of the different layers on $V_{th}$ should take into account the ionic strength of the solution, since the studied layer charge and dipole may reside beyond the Debye screening length, $\lambda_D$,[24] and thus may be screened and will not be sensed by the device (Figure 1a).[25] Control over $\lambda_D$ was achieved by a series of dilutions of the phosphate buffer. Evidently, $V_{th\text{-}BG}$ remains constant regardless of $\lambda_D$ for the bare device due to the close proximity of the charged groups and dipoles to the oxide surface (Figure 4b). A large shift in $V_{th}$ is observed following APTMS absorption, as will be discussed below. However, only a small dependence on $\lambda_D$ is observed, with $V_{th\text{-}BG}$ slightly decreasing with increasing $\lambda_D$. This is because the entire layer resides within the Debye screening region for the entire experimental ionic strengths (Figure 1a). No significant shift in $V_{th\text{-}BG}$ was obtained after the addition of a biotin layer for $\lambda_D$ = 0.8 nm for which this layer's charge and dipole is screened. Indeed, increasing the screening length to 2.4 nm results in a significant decrease in $V_{th\text{-}BG}$. This effect becomes even more pronounced upon further increasing the screening length. Similarly, the adsorption of streptavidin also results in an increase in $V_{th\text{-}BG}$, which becomes more significant at larger $\lambda_D$. While the overall observed changes seem to be smaller than the experimental error, we note that this error reflects variations in the behavior of different devices. In fact the same trends were observed in each of the measured devices, with a shift between different devices.

The potential drop across the different layers adsorbed on the surface was estimated from their induced changes on the threshold voltage (Table 1). For each layer $\Delta\Psi_{0_i}$ was calculated by eq 7 with PZC values before and after the layer deposition obtained from contact angle studies in similar systems,[38] and the experimental sensitivity values (Figure 3a). These values were then inserted into eq 6 yielding $\Psi_{OL_i}$. A value of *ca.* −300 mV was found for $\Psi_{OL}$ for the APTMS layer ($\lambda_D$ = 0.8 nm). This value is much smaller than the 1 V value obtained for similar structures under dry conditions,[26] probably due to screening effects. Indeed, several studies of the changes in devices' flat band voltage (and the threshold voltage) due to adsorption of organic layers showed values ranging between zero[27,28] and tens of millivolts[29,30] in electrolyte solution. We note that an

**TABLE 1. Contribution of Organic Layers to Changes in Threshold Voltage**

| | APTMS | | | biotin | | | streptavidin | | |
|---|---|---|---|---|---|---|---|---|---|
| $\lambda_D$ (nm) | $\Delta V_{th\text{-}BG}$[a] (V) | $\Delta\Psi_0$[b,c] (mV) | $\Psi_{OL}$ (mV) | $\Delta V_{th\text{-}BG}$[a] (V) | $\Delta\Psi_0$[b,c] (mV) | $\Psi_{OL}$ (mV) | $\Delta V_{th\text{-}BG}$[a] (V) | $\Delta\Psi_0$[b,c,d] (mV) | $\Psi_{OL}$ (mV) |
| 0.8 | −3 ± 0.5 | 180 | −300 ± 30 | 0.25 ± 1.7 | [f] | [f] | −0.1 ± 3.5 | [f] | [f] |
| 2.4 | [e] | | | −6 ± 1.2 | −150 | −90 ± 25 | 0.8 ± 2.1 | 200 | −170 ± 80[g] |
| 3.5 | [e] | | | −13 ± 1 | −170 | −360 ± 100 | −1.95 ± 0.9 | 200 | −120 ± 60[g] |

[a]Calculated by the threshold voltage difference due to layer adsorption (Figure 4b). [b]Averaged values, calculated from eq 8 using sensitivity factors obtained in Figure 3a and the experimental front-back coupling factor (=25). Errors evaluated by the minimal and maximal calculated values. [c]PZC values of 8 for APTMS, 2 for $SiO_2$, and 3.5 for biotin were used, according to values obtained by contact angle measurements on similarly prepared surfaces.[38] [d]Streptdavidin PZC of 7 estimated by the protein isoelectric point. [e]Not evaluated due to irreproducibility of measurements of the activated surface. [f]Not calculated due to small $V_{th}$ shift. [g]The large error reflects variations in the experimental results, and uncertainty in the PZC values which might differ from the protein isoelectric point once adsorbed on the surface.

overall large shift of the curve toward higher $V_{BG}$ values was observed following APTMS modification (inset of Figure 4). This is mainly due to the formation/occupation of interface states at the top oxide−silicon interface with negative charge during the exposure of the surface to UV irradiation during the activation treatment.[31] This large effect, together with the fact that the activated surface is less stable and shows larger variation in the $I_{DS}-V_{BG}$ relations, may greatly limit the accuracy of the calculated $\Psi_{OL}$ value for this layer. We note that current experiments on a similar system show that this charging effect can be eliminated by using an acidic (piranha) cleaning/activation treatment (Y. Rosenwaks, personal communication).

The calculations of the biotin layer contribution to the shifts on $V_{th\text{-}BG}$ were conducted only for the larger screening lengths ($\lambda_D$ = 2.4 and 3.5 nm) since at these conditions the layer's charge and dipole contribute more effectively to the signal. The −90 ± 25 mV potential drop across the biotin layer for $\lambda_D$ = 2.4 nm is in agreement with the value reported by Taylor *et al*. for measurements in dry conditions.[32] For $\lambda_D$ = 3.5 nm the potential drop across the layer decreases to a value of −360 ± 100 mV. This larger potential drop across the layer is attributed to lesser screening obtained for this lower ionic strength solution. Smaller changes in $V_{th\text{-}BG}$ were measured after the adsorption of the streptavidin layer even for $\lambda_D$ = 3.5 nm, for which the charge and dipole should not be completely screened. This small effect is a result of the opposite contribution of the PZC change and the potential difference across the layer (Table 1). These results highlight the different effects of organic layer on device performance. Such effects may be modulated by external conditions such as the solution ionic strength and pH. In this respect we note that the measurements were carried out in solutions with pH value of 7, close to the protein's isoelectric point at which the protein is only slightly charged.[33] Changing the pH of the solution may increase the contribution of the potential across the layer, thus increasing the overall signal. Indeed, measurements done at higher pH solutions have shown an increase in the threshold voltage (data not shown), manifesting a decrease in the protein effective charge.[11,13]

**The Transistor Gain, $gm_f$.** The main characteristics of the detection capacity of a bio-FET device is its inherent sensitivity to surface charge or surface potential, which can be quantified by the transistor gain. The gain performance of the bio-FET in solution can be quantified by replacing the gate voltage by $V_{ref}$ in the traditional transistor gain definition, yielding: $gm_f = dI_{DS}/dV_{ref}$. For the linear (strong inversion) region ($V_{ref} - V_{th\text{-}f} \gg V_{DS}$), the gain is thus given by[34]

$$gm_f = \frac{C_{eff}\mu V_{DS} W}{L} \qquad (9)$$

where $C_{eff}$ is the effective capacitance of the top dielectric, the organic layers, and the solution, $\mu$ is the silicon mobility, $V_{DS}$ is the drain-source voltage, and $W$ and $L$ are the width and length of the conducting channel, respectively. The experimental results show that $gm_f$ decreases after each modification (Figure 5). This decrease seems to be more pronounced upon the addition of more layers to the device's gate. From eq 9 it is evident that the reduction in $gm_f$ can be attributed to changes in $C_{eff}$ due to the addition of organic layers. $C_{eff}$ was evaluated using a simple model of ideal plate capacitors in series (Figure 5). Indeed, $C_{eff}$ and $gm_f$ show the same trends during the construction of the device layers, with slight discrepancies between these trends, probably due to additional capacitive effects. These results clearly demonstrate the capacitive effect of the layers on device performance. These effects should be considered in the design of a bio-FET, and the quantification of its performance.

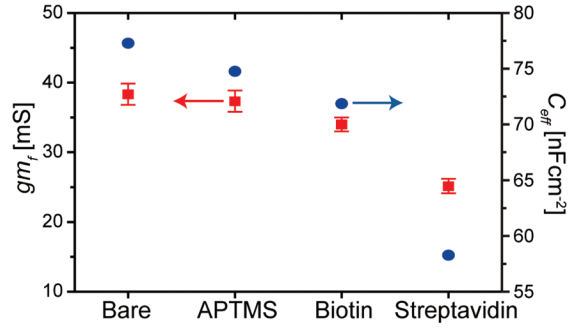


**Figure 5. Device gain behavior. Experimental gain, $gm_f$ (red squares), and calculated capacitance (blue circles), for the different gate layers ($\lambda_D$ = 2.43 nm, $V_{BG}$ = 20 V). Capacitance was calculated using a simple model of ideal plate capacitors in series, using the manufacturer stated thickness values and dielectric constants of 3.5 and 11.2 for silicon-oxide and silicon, respectively. The solution capacitance was calculated from the diffused layer capacitance.[22] The capacitance of the organic layers was estimated using thicknesses obtained from ellipsometry measurements, a dielectric constant of 2.4 for the APTMS layer,[38] and estimated value of 2.3 for both the biotin and streptavidin layers.**

## SUMMARY AND CONCLUSION

The evolution of $I-V$ relations of fully depleted SOI FET devices following modifications of their floating gate with APTMS, biotin, and streptavidin, as a model system for biosensing applications, was characterized in wet environment and with varying ionic strength. The pH sensitivity of the devices was shown to vary during the construction of the different organic layers owing to changes in the number and nature of amphoteric groups on the surface. The sensitivity was reduced following the construction of the APTMS and biotin layers. Increased pH sensitivity was observed at low ionic strengths once the streptavidin was attached to the surface due to its amine and carboxylic side chains.

The dependence of the threshold voltage on the electrolyte screening length was studied for each layer of the device. Only a small dependence of the threshold

voltage on the electrolyte Debye screening length was observed after the deposition of the first APTMS layer. This is because the thickness of this layer is smaller than the screening length for the entire measurement range. Consequently, a larger threshold voltage dependence on the screening length was observed for the biotin and streptavidin layers. A one-dimensional electrostatic model was used in order to analyze the combined effects of the constructed layers, and the electrolyte on the device threshold voltage. Using this model the different contributions of the organic layers both *via* dipolar effects and changes in the surface PZC, were analyzed. These two effects were found to be accumulative for the APTMS and biotin layers. However, for the streptavidin layers these effects showed an opposite trend. In addition to these effects the channel gain is also affected by the organic layers due to their dielectric nature which changes the effective capacitance of the system, resulting in reduction of the gain following the formation of each of the organic layers of the device. These results demonstrate the multiple effects of the organic layers on the performance of FET devices. These effects should be considered in the design and clinical applications of such devices.

## METHODS

**Device Gate Modification by Construction of Bio-Organic Layers.** Fully depleted enhancement mode SOI n-channel MOSFET devices (contributed by Intel Research Lab, Jerusalem, Israel)[35] were used (Figure 1a). To achieve the full-depletion condition devices consisted of 1 μm buried oxide (BOX), a 30−40 nm SOI with resistivity of 5−10 Ω · cm (corresponding to a boron concentration of about $10^{15}$ $cm^{-3}$), and a 20−50 nm top gate dielectric.[36] Source and drain electrodes were fabricated from aluminum in order to ensure ohmic contacts, and covered by gold.

Prior to modification, the devices were cleaned by immersion in ethanol and drying. Devices were then treated in a UV ozone cleaning system (T10 × 19-OES, UVOCS, USA) for 45 min in order to increase the surface density of the hydroxyl groups. This was followed by a heat treatment at 100 °C for 30 min on a hot-plate. The activated devices were immediately immersed in an APTMS solution (95% ethanol, 5% APTMS) for 10−12 min, followed by thorough rinsing in ethanol and three times in triple-distilled water (TDW). Devices were dried under $N_2$ and heat treated at 100−120 °C for 30 min to remove all excess ethanol and water, and establish covalent bonding of the silane.

For the formation of the biotin layer, APTMS covered devices were immersed in 10 mM biotin−NHS in phosphate buffer (pH = 7.2) overnight. Since biotin−NHS does not dissolve in the buffer it was first dissolved in dimethylformamide (DMF) and then diluted in the phosphate buffer to the final concentration such that the amount of DMF did not exceed 10% of the final volume.[37] While the solution appeared as a hazy suspension, indicating incomplete solubility, the reaction was effectively completed. After biotin assembly, devices were washed in DMF, buffer, and TDW followed by drying under $N_2$ stream. For streptavidin conjugation, biotinated devices were exposed to a freshly prepared solution of streptavidin (5 μM in 10 mM sodium phosphate buffer, pH 7) for 3−4 h. Devices were then washed in the same buffer solution and under TDW stream three times (using a syringe) and dried under a $N_2$ stream.

The layers were characterized following each modification step using ellipsomerty (SE800, Sentech Instruments GmbH, Germany). Further characterization of the chemical properties and morphology included contact angle, X-ray photoelectron spectroscopy, and atomic force microscopy. For these measurements layers were deposited on bare p-type Si wafers (boron concentration of about $10^{15}$ $cm^{-3}$, ρ ≈ 10 Ω · cm) covered with layers of thermal oxide (50 −1250 Å).

**Electrical Device Characterization.** Electrical device characterizations were acquired in solution (phosphate buffered saline (PBS), pH = 7.4), on a four-terminal measurement setup as shown in Figure 1a, using a semiconductor parameter analyzer (model 4155C, Agilent Technologies, USA). Ag/AgCl electrode (Metrohm, Switzerland) immersed in the buffer was used as a reference electrode. $V_{ref}$ was restricted to values lower than ±2 V in order to eliminate electrode deterioration, gate dielectric electrical breakdown, or other electrochemical reactions in solution. $V_{BG}$ was varied between −20 and +80 V, and $V_{DS}$ was set at +0.1 V in all the experiments. Characterizations were obtained for the same device following each gate modification step including cleaning in ethanol, UV-ozone activation, and after modifications with APTMS, biotin, and streptavidin. In each experiment both $I_{DS}-V_{BG}$ (with varying $V_{ref}$) and $I_{DS}-V_{ref}$ (with varying $V_{BG}$) were measured, showing the same behavior as discussed in the text (Figure 2b). Study of the effect of the ionic strength and screening length was achieved by successive buffer dilutions relative to 1X PBS (150 mM NaCl, 3 mM KCl, and 10 mM phosphate salts (monobasic and dibasic)), and characterization after each dilution. In order to verify the reproducibility of our results after completing the measurements $I-V$ curves were remeasured at 1X PBS. For the calculations of the pH sensitivity, the same $I-V$ curves were measured at pH 5, 7, and 9 for each of the ionic strengths. The pH sensitivity was calculated by $\Delta V_{th}/\Delta$pH using either $V_{th\text{-}ref}$ or $V_{th\text{-}BG}$. An average value was obtained by considering the pH sensitivities obtained for each pair of measurements at two different pH conditions (a total of three values). For the bare surface, APTMS, and biotin layers the pH sensitivity was compared to values obtained by the procedure used in ref 23, and similar values were obtained. $V_{th}$ was obtained from the intercept of the linear extrapolation of the $I-V$ curve in the linear regime with the voltage axis since small $V_{DS}$ values were used in the measurements.

*Acknowledgment.* This research was supported by the CT program of the ISF (Grant No. 1717/07), and Intel Corporation research grant. We thank Drs. Gil Shalev and Ilan Levy from Intel Research Lab, Israel, for fruitful discussions.

## REFERENCES AND NOTES

1. *Handbook of Biosensors and Biochips*; Marks, R. S., Cullen, D. C., Karube, I., Lowe, C. R., Weetall, H. H., Eds.; Wiley: New York, 2007; Vol. 1.
2. Xu, J. J.; Luo, X. L.; Chen, H. Y. Analytical Aspects of FET-Based Biosensors. *Front. Biosci.* **2005**, *10*, 420–30.
3. Cohen, R.; Kronik, L.; Shanzer, A.; Cahen, D.; Liu, A.; Rosenwaks, Y.; Lorenz, J. K.; Ellis, A. B. Molecular Control Over Semiconductor Surface Electronic Properties: Dicarboxylic Acids on CdTe, CdSe, GaAs, and InP. *J. Am. Chem. Soc.* **1999**, *121*, 10545–53.
4. Cahen, D.; Naaman, R.; Vager, Z. The Cooperative Molecular Field Effect. *Adv. Funct. Mater.* **2005**, *15*, 1571–8.
5. Natan, A.; Kronik, L.; Haick, H.; Tung, R. T. Electrostatic Properties of Ideal and Nonideal Polar Organic Monolayers: Implications for Electronic Devices. *Adv. Mater.* **2007**, *19*, 4103–17.
6. Schoening, M. J.; Poghossian, A. Recent Advances in Biologically Sensitive Field-Effect Transistors (BioFETs). *Analyst* **2002**, *127*, 1137–51.
7. Landheer, D.; Aers, G.; McKinnon, W. R.; Deen, M. J.; Ranuarez, J. C. Model for the Field Effect from Layers of Biological Macromolecules on the Gates of Metal-Oxide-Semiconductor Transistors. *J. Appl. Phys.* **2005**, *98*, 044701.
8. Poghossian, A.; Cherstvy, A.; Ingebrandt, S.; Offenhaeusser,

A.; Schoening, M. J. Possibilities and Limitations of Label-Free Detection of DNA Hybridization with Field-Effect-Based Devices. *Sens. Actuator B* **2005**, *111*, 470–80.
9. Gozlan, N.; Haick, H. Coverage Effect of Self-Assembled Polar Molecules on the Surface Energetics of Silicon. *J. Phys. Chem. C* **2008**, *112*, 12599–601.
10. Patolsky, F.; Zheng, G.; Hayden, O.; Lakadamyali, M.; Zhuang, X.; Lieber, C. M. Electrical Detection of Single Viruses. *Proc. Natl. Acad. Sci. U.S.A.* **2004**, *101*, 14017–22.
11. Patolsky, F.; Zheng, G.; Lieber, C. M. Nanowire Based Biosensors. *Anal. Chem.* **2006**, *78*, 4260–9.
12. Star, A.; Gabriel, J. C. P.; Bradley, K.; Gruner, G. Electronic Detection of Specific Protein Binding Using Nanotube FET Devices. *Nano Lett.* **2003**, *3*, 459–63.
13. Stern, E.; Klemic, J. F.; Routenberg, D. A.; Wyrembak, P. N.; Turner-Evans, D. B.; Hamilton, A. D.; LaVan, D. A.; Fahmy, T. M.; Reed, M. A. Label-Free Immunodetection with CMOS-Compatible Semiconducting Nanowires. *Nature* **2007**, *445*, 519–22.
14. Fung, C. D.; Cheung, P. W.; Ko, W. H. A Generalized Theory of an Electrolyte-Insulator-Semiconductor Field-Effect Transistor. *IEEE Trans. Electron Devices* **1986**, *33*, 8–18.
15. Takulapalli, B. R. Molecular Sensing Using Monolayer Floating Gate, Fully Depleted SOI MOSFET Acting as an Exponential Transducer. *ACS Nano* **2010**, *4*, 999–1011.
16. Shalev, G.; Doron, A.; Virobnik, U.; Cohen, A.; Sanhedrai, Y.; Levy, I. Gain Optimization in Ion Sensitive Field-Effect Transistor Based Sensor with Fully Depleted Silicon on Insulator. *Appl. Phys. Lett.* **2008**, *93*, 083902−3.
17. Young, K. K. Analysis of Conduction in Fully Depleted SOI MOSFETs. *IEEE Trans. Electron Devices* **1989**, *36*, 504–6.
18. Bousse, L. Single Electrode-Potentials Related to Flat-Band Voltage Measurements on EOS and MOS Structures. *J. Chem. Phys.* **1982**, *76*, 5128–33.
19. Siu, W. M.; Cobbold, R. S. C. Basic Properties of the Electrolyte−$SiO_2$−Si System—Physical and Theoretical Aspects. *IEEE Trans. Electron Devices* **1979**, *26*, 1805–15.
20. Waleed Shinwari, M.; Jamal Deen, M.; Landheer, D. Study of the Electrolyte−Insulator−Semiconductor Field-Effect Transistor (EISFET) with Applications in Biosensor Design. *Microelectron. Reliab.* **2007**, *47*, 2025–57.
21. Martinoia, S.; Massobrio, G.; Lorenzelli, L. Modeling ISFET Microsensor and ISFET-Based Microsystems: A Review. *Sens. Actuators, B* **2005**, *105*, 14–27.
22. Van Hal, R. E. G.; Eijkel, J. C. T.; Bergveld, P. A General Model to Describe the Electrostatic Potential at Electrolyte Oxide Interfaces. *Adv. Colloid Interface Sci.* **1996**, *69*, 31–62.
23. Shalev, G.; Halpern, E.; Doron, A.; Cohen, A.; Rosenwaks, Y.; Levy, I. Surface Chemical Modification Induces Nanometer Scale Electron Confinement in Field Effect Device. *J. Chem. Phys.* **2009**, *131*, 024702 1−6.
24. Israelachvili, J. *Intermolecular & Surface Forces*, 2nd ed.; Academic Press: New York, 1991.
25. Stern, E.; Wagner, R.; Sigworth, F. J.; Breaker, R.; Fahmy, T. M.; Reed, M. A. Importance of the Debye Screening Length on Nanowire Field Effect Transistor Sensors. *Nano Lett.* **2007**, *7*, 3405–9.
26. Shaya, O.; Shaked, M.; Usherenko, Y.; Halpern, E.; Shalev, G.; Doron, A.; Levy, I.; Rosenwaks, Y. Tracing the Mechanism of Molecular Gated Transistors. *J. Phys. Chem. C* **2009**, *113*, 6163–8.
27. Allongue, P.; Henry de Villeneuve, C.; Pinson, J. Structural Characterization of Organic Monolayers on Si ⟨111⟩ from Capacitance Measurements. *Electrochim. Acta* **2000**, *45*, 3241–8.
28. Einati, H.; Mottel, A.; Inberg, A.; Shacham-Diamand, Y. Electrochemical Studies of Self-Assembled Monolayers Using Impedance Spectroscopy. *Electrochim. Acta* **2009**, *54*, 6063–9.
29. Jin, Z. H.; Vezenov, D. V.; Lee, Y. W.; Zull, J. E.; Sukenik, C. N.; Savinell, R. F. Alternating Current Impedance Characterization of the Structure of Alkylsiloxane Self-Assembled Monolayers on Silicon. *Langmuir* **1994**, *10*, 2662–71.
30. Bansal, A.; Lewis, N. S. Electrochemical Properties of (111)-Oriented *n*-Si Surfaces Derivatized with Covalently-Attached Alkyl Chains. *J. Phys. Chem. B* **1998**, *102*, 1067–70.
31. Nicollian, E. H.; Brews, J. R. *MOS Physics and Technology*; Wiley: New York, 1982.
32. Taylor, D. M.; Morgan, H.; D'Silva, C. Characterization of Chemisorbed Monolayers by Surface Potential Measurements. *J. Phys. D: Appl. Phys.* **1991**, *24*, 1443–50.
33. Aslan, K.; Perez-Luna, H. Surface Modification of Colloidal Gold by Chemisorption of Alkanethiols in the Presence of Nonionic Surfactant. *Langmuir* **2002**, *18*, 6059–65.
34. Sze, S. M. *Semiconductor Devices—Physics and Technology*, 2nd ed.; Wiley: New York, 2002.
35. Shalev, G.; Cohen, A.; Doron, A.; Machauf, A.; Horesh, M.; Virobnik, U.; Ullien, D.; Levy, I. Standard CMOS Fabrication of a Sensitive Fully Depleted Electrolyte−Insulator−Semiconductor Field Effect Transistor for Biosensor Applications. *Sensors* **2009**, *9*, 4366–79.
36. Sakurai, T.; Matsuzawa, A.; Douseki, T. *Fully-Depleted SOI CMOS Circuits and Technology for Ultralow-Power Applications*, 1st ed.; Springer: New York, 2006.
37. Hermanson, G. T. *Bioconjugate Techniques*; Academic Press: San Diego, 1996.
38. Halpern, E. Capacitance−Voltage Characterization of Chemically Functionalized Silicon-Insulator-Electrolyte Systems., Tel Aviv University, 2009.